



# Quantitative Phase Retrieval Through Scattering Medium via Compressive Sensing

Tong Peng , Runze Li, Junwei Min , Dan Dan , Meiling Zhou , Xianghua Yu , Chunmin Zhang, Chen Bai , and Baoli Yao 

**Abstract**—Scattering media, such as biological tissues and turbid liquids, scatter light randomly and introduce several challenges when imaging objects behind them. The transmission matrix (TM) describes the relation between the input and output of a beam transmitted through a medium, which can be used to reconstruct a target located behind a scattering medium. However, the current TM methods cannot easily retrieve the phase distribution of objects inside or behind a scattering medium. In this work, a compressive sensing (CS) method to identify the TM of a scatter contained in an imaging system was investigated. By calibrating the TM, the phase information of the object can be retrieved quantitatively. This method allows one to retrieve multilevel and dynamic phase objects behind different scatters. The influence of the calibration parameters on the reconstruction quality was investigated in detail. The proposed method, featuring noninterference measurements of the TM and exploiting a large field of view, can be used in phase imaging applications.

**Index Terms**—Imaging through scattering media, phase retrieval, transmission matrix, compressive sensing.

## I. INTRODUCTION

RESEARCH on focusing and imaging through a scattering medium has recently triggered substantial interest [1]–[3] due to its important applications in biomedical imaging, fire rescue, micromanipulation, etc. [4]–[7]. Thus far, many

Manuscript received August 19, 2021; revised November 19, 2021; accepted December 15, 2021. Date of publication December 17, 2021; date of current version December 29, 2021. This work was supported in part by the National Natural Science Foundation of China under Grants 61905277, 61991452, and 61705256, in part by the Key Research and Development Projects of Shaanxi Province under Grant 2020GY-008, and in part by the Youth Innovation Promotion Association, CAS under Grant 2021401. (Corresponding authors: Chen Bai; Baoli Yao.)

Runze Li, Junwei Min, Dan Dan, Meiling Zhou, Xianghua Yu, and Chen Bai are with the State Key Laboratory of Transient Optics and Photonics, Xi'an Institute of Optics and Precision Mechanics, Chinese Academy of Sciences, Xi'an 710119, China (e-mail: lirunze@opt.cn; mjw@opt.ac.cn; dandan@opt.ac.cn; zhoulmeiling@opt.ac.cn; yxh@opt.cn; baichen@opt.ac.cn).

Tong Peng is with the State Key Laboratory of Transient Optics and Photonics, Xi'an Institute of Optics and Precision Mechanics, Chinese Academy of Sciences, Xi'an 710119, China, with the University of Chinese Academy of Sciences, Beijing 100049, China, and also with the School of Science, Xi'an Jiaotong University, Xi'an 710049, China (e-mail: pengtong@opt.ac.cn).

Chunmin Zhang is with the School of Science, Xi'an Jiaotong University, Xi'an 710049, China (e-mail: zcm@xjtu.edu.cn).

Baoli Yao is with the State Key Laboratory of Transient Optics and Photonics, Xi'an Institute of Optics and Precision Mechanics, Chinese Academy of Sciences, Xi'an 710119, China, with the University of Chinese Academy of Sciences, Beijing 100049, China, and also with the National Laboratory for Marine Science and Technology (Qingdao), Qingdao 266200, China (e-mail: yaobl@opt.ac.cn).

Digital Object Identifier 10.1109/JPHOT.2021.3136509

approaches for imaging through a scattering medium, such as wavefront shaping [8], speckle correlation [9], and optical gating [10], have been developed. However, most of these techniques rely on the “memory effect” [11] of the scattering medium, resulting in a relatively small field of view (FOV). Moreover, by assuming that the scattering medium can be approximated by a phase insensitive “scattering lens”, the proposed techniques can only recover the intensity distribution of the object, leaving the phase information behind [12]. Since the phase intrinsically reflects the topography, internal structures, composition, and many other characteristics of the object [13]–[15], retrieving the phase distribution of the object behind the scattering medium is essential and meaningful.

A number of methods, such as phase conjugation [16], [17], digital holography [18]–[20], and transmission matrix (TM) [21]–[25], have been investigated to achieve phase retrieval. These methods do not rely on the memory effect of the scattering media, which can achieve a relatively large FOV in imaging. Specifically, with the phase conjugation method, qualitative phase information can be reconstructed by applying the conjugated phase of the distorted wavefront to a spatial light modulator (SLM) to refocus or image the object behind the scattering medium [16]. Digital holography can recover the complex amplitude of the target quantitatively via speckle interferometry [20]. However, this method requires a reference beam and is limited by vibrations or system perturbations, similar to other interference setups, resulting in time consumption, a low signal-to-noise ratio (SNR), and limited accuracy of quantitative phase retrieval. TM describes the relation between the input and the output of the light transmitted through a medium, and the complex input light field can be retrieved if both the TM of the system and the output field can be determined.

With the development of phase retrieval algorithms, the TM of a system with its scattering medium can be obtained by loading a series of calibrated phase images into a modulator and capturing the corresponding speckle patterns. For instance, by combining a digital micromirror device (DMD) and double phase retrieval (DPR), the TM of an imaging system can be learned effectively. This method, featuring robust and avoiding interferometric measurements, can realize refocusing of light through scattering media [26], [27]. After that, objects behind scattering media can also be estimated by the following developed DPR methods with enhanced resolution and SNR [28]–[30]. Although such methods have been proven to be a useful strategy to recognize inverse scattering, challenges still exist.

First, previous studies that utilize the DPR method are often limited to the estimation of TM with binary input (binary-TM), regardless of whether it is based on a digital micromirror device (DMD) or spatial light modulator (SLM), leading to the lack of quantitative information in the subsequent imaging of objects. In addition, in most TM-based methods, the objects to be recovered are still “virtual objects” that are generated by the SLM or DMD, rather than practical items with specific optical thicknesses. Indeed, without quantitative information, the application of this method is relatively limited. In addition, in most of these studies, using the DPR to recover objects behind scattering media requires massive amounts of computation and millions of CPU hours, and the computing speed is limited. Fortunately, the latest algorithms based on compressive sensing (CS), the phase retrieval vector-approximate message passing algorithm (prVAMP) [31], [32], are proposed with greatly accelerated processing and a relatively high SNR, which can bring great convenience for further investigating the optimization of other TM-based imaging. However, like the other DPR method, prVAMP also uses binary patterns as the input to acquire a binary-TM, and the ability of quantitative phase retrieval is absent.

To address these issues, in this work, a new method based on the prVAMP, in which the TM beyond the binary input can be obtained by capturing a series of calibrated images with different phases, i.e., the calibrated-TM, is proposed. The method is a development of the prVAMP, which retains the features of non-interference measurements and fast and high-quality imaging with large FOVs. Moreover, the quantitative phase information of the target behind the scattering medium can be effectively reconstructed, thereby extending the potential applications in the field of TM-based imaging. By retrieving multilevel phase objects and the dynamic phase steps behind different scatters, the influences of the calibration parameters and reconstruction quality were investigated in detail.

## II. PRINCIPLE AND EXPERIMENT

### A. Principle of the Method

In an optical imaging system illuminated by coherent light and containing a scattering medium, the relation between the object wavefront (input) and the detected speckle field (output) can be connected via the TM as follows:

$$Y = AX + \mathbf{E} \quad (1)$$

Here,  $\mathbf{X}$  denotes the input light field,  $\mathbf{Y}$  represents the output light field,  $\mathbf{A}$  corresponds to the TM of the system, and  $\mathbf{E}$  represents the noise. Generally, a detection camera can only capture the information about the light intensity. Therefore, the measurement process can be written as follows:

$$Y^2 = |AX + \mathbf{E}|^2 \quad (2)$$

In real-life applications, the square root of the intensity is generally considered:

$$Y = |AX + \mathbf{E}| \quad (3)$$

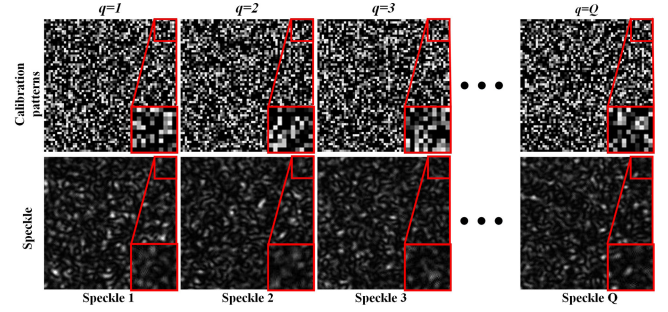


Fig. 1. Actual calibration patterns and the corresponding speckles, the insets illustrate the detailed information of the calibration patterns.

To obtain the TM of the scatter with calibrated information and quantitatively retrieve the phase of the object, a double phase retrieval method can be used.

*Original Binary-TM Measurement:* The TM is measured by loading a series of calibration phase patterns. One specific calibration pattern sent to the SLM can be depicted as  $\mathbf{x}_q \in \mathbb{R}^{N^2 \times 1}$  with  $q = 1, \dots, Q$ . Here,  $N^2$  denotes the pixel number of the calibration phase, whereas  $Q$  corresponds to the number of calibrated patterns. The corresponding measurement of the speckle pattern is  $\mathbf{y}_q \in \mathbb{R}^{M^2 \times 1}$ , where  $M^2$  refers to the pixel number of the speckle pattern. The camera transforms the pattern into  $\mathbf{y}_q = |\mathbf{A}\mathbf{x}_q + \mathbf{e}_q|$  via the TM  $\mathbf{A} \in \mathbb{C}^{M^2 \times N^2}$ . For all calibration patterns,  $\mathbf{X} = [x_1, x_2, \dots, x_q] \in \mathbb{R}^{N^2 \times Q}$ ,  $\mathbf{Y} = [y_1, y_2, \dots, y_q] \in \mathbb{R}_+^{M^2 \times Q}$ ,  $\mathbf{E} = [\mathbf{e}_1, \mathbf{e}_2, \dots, \mathbf{e}_q] \in \mathbb{C}^{M^2 \times Q}$ .

By taking their transpose, the patterns can be written as follows:

$$\mathbf{Y}^H = |\mathbf{X}^H \mathbf{A}^H + \mathbf{E}^H| \quad (4)$$

For the  $m^{\text{th}}$  element of  $\mathbf{Y}$  one obtains:

$$\mathbf{y}_m^H = |\mathbf{X}^H \mathbf{a}_m^H + \mathbf{e}_m^H| \quad (5)$$

Here,  $\mathbf{a}_m^H$  and  $\mathbf{e}_m^H$  denote the  $m^{\text{th}}$  row of  $\mathbf{A}$  and  $\mathbf{E}$ , respectively. In contrast with traditional methods, the elements of  $\mathbf{X}^H$  are designed to follow a Bernoulli distribution with probability  $p = 0.5$ . This implies that each element of  $\mathbf{X}^H$  is either zero or positive items with a probability of 0.5.

*Calibrated-TM Measurement:* In this work, a different strategy is proposed. The binarization process used in the SLM has been proven to efficiently measure the TM. However, performing phase retrieval with this approach does not provide a quantitative result. For this reason, only phase maps with binary values, except for noise, have been used in previous studies. In this work, a more elaborate design of  $\mathbf{X}^H$  was introduced. Initially, half elements of calibration signals are randomly selected to be zeros or positive items, i.e., the random pixels of the positive items follow a Gaussian distribution. Then, the phase of the positive elements is randomly substituted with the uniform  $[0, 1]$  distribution. Actual calibration patterns and their corresponding measurements are illustrated in Fig. 1. This new strategy satisfies both the sparsity of CS and the quantitative measurement of TM.

In fact, the central challenge to using the double phase retrieval method in practice is the computational time. Therefore, in this work, we utilized the developed algorithm, phase retrieval vector

approximate message passing (prVAMP) [31], which offers satisfactory accuracy while running hundreds of times faster with potentially parallel processes and acceleration by GPUs. prVAMP is a special case of the recently developed generalized vector approximate message passing (GVAMP) algorithm [33]. This is a typical algorithm for computing approximate minimum means squared error (MMSE) or maximum a posteriori (MAP) solution to inverse problems involving generalized linear measurements (GLMs); defined to be any measurement of the form

$$\mathbf{y} = F(\mathbf{z} + \mathbf{w}) \text{ with } \mathbf{z} = \Phi \mathbf{x} \quad (6)$$

where  $\Phi$  is our measurement matrix (which is a known pattern  $\mathbf{X}^H$  when calibrating the TM),  $\mathbf{x}$  is our signal of interest,  $\mathbf{w}$  is noise, and  $F(\cdot)$  denotes a simple nonlinear procedure, also known as the generalized linear model, which evolved from CS [33]. Moreover, the elaborate measurement matrix represents the coefficients that are randomly selected by the Gaussian random matrix, which satisfies the condition of compressive sensing methodology to ensure the measurements have a high probability of including enough information to enable TM reconstruction with small or zero errors [31]. As a result, prVAMP is designed for the special case  $F(\cdot) = |\cdot|$ , which is a Bayesian algorithm that requires priors on the distribution of the signal and noise.

Specifically, prVAMP works by first splitting the vectors  $\mathbf{x}$  and  $\mathbf{z}$  into two sets of identical vectors  $\mathbf{x}_1$  and  $\mathbf{x}_2$  and  $\mathbf{z}_1$  and  $\mathbf{z}_2$ . Iterations of the algorithm then broadly consist of four steps [32]. First, there are **two** “denoising” steps that impose priors on  $\mathbf{x}$  and  $\mathbf{z}$  and ensure that they are consistent with the measurements  $\mathbf{y}$ . Then, there are **two** linear minimum mean squared error (LMMSE) estimation steps that ensure that the estimates of  $\mathbf{x}$  and  $\mathbf{z}$  are consistent with each other.

*Quantitative phase retrieval:* If  $Q$  is sufficiently large ( $Q > 4N^2$ ), each  $\mathbf{a}_m^H$  and  $\mathbf{y}_m^H$  row of  $\mathbf{X}^H$  can be obtained by applying the GPU-accelerated prVAMP [31]. This avoids difficulties in collecting an interferometric measurement with time-consuming computation. Once the calibrated TM of the system is measured, the quantitative phase information of objects can be readily obtained from Eq. (3).

### B. Experimental Setup

The experimental setup for quantifying the phase retrieval through a scattering medium is shown in Fig. 2. A laser beam ( $\lambda = 532 \text{ nm}$ ) passes through a reversed telescope (L1,  $f_1 = 50 \text{ mm}$ ; L2,  $f_2 = 150 \text{ mm}$ ) for beam expansion. The expanded beam is projected onto a phase-only SLM (1920×1080 pixels, pixel pitch  $8 \mu\text{m}$ , PLUTO-VIS, HoloEye Inc., Germany) to generate the calibrated patterns and virtual targets. The modulated light is then directed onto the target plane via an imaging system (L3,  $f_3 = 200 \text{ mm}$ ; L4,  $f_4 = 20 \text{ mm}$ ). In other words, the image of the SLM overlaps with the target. The target and the calibration pattern are finally imaged onto a CCD camera (1280×960 pixels, pixel pitch  $3.75 \mu\text{m}$ , 8 bit, DMK 23U445, The Imaging Source Inc., Germany) via a 20X objective lens (Obj, 20X, NA0.45, Nikon Inc., Japan) and a tube lens (L5,  $f_5 = 200 \text{ mm}$ ). In contrast, in terms of the experiment with a real phase target, the specimen is directly located at the object plane,

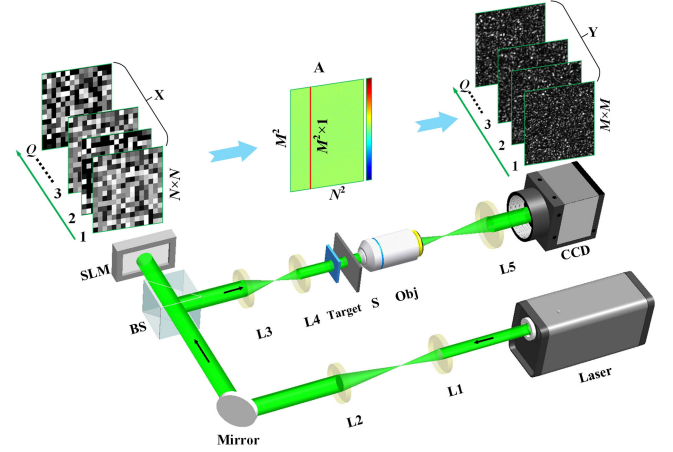


Fig. 2. Principle and experimental setup to achieve quantitative phase retrieval through a scattering medium. L1-L5, lenses, BS, beam splitter, SLM, Spatial light modulator, Obj, objective lens, and S, scattering medium.

and the SLM is utilized as a mirror without any modulation. A scattering medium consisting of ground glass (10DKIT-C2, Newport Inc., USA) is placed between the target and objective lens.

In this study, the centered  $240 \times 240$  pixels of SLM are used to generate the calibration patterns, and they are grouped into  $60 \times 60$  segments, each of which is composed of  $4 \times 4$  pixels. The  $960 \times 960$  pixels of the CCD are used to capture the speckle pattern, but in the data processing, the  $960 \times 960$  pixels are resized to  $256 \times 256$ . The data were finally transferred and processed by a computer equipped with an E5-2690 CPU (Intel Corporation, USA), 128 GB memory and double NVIDIA Titan V GPUs (Nvidia Corporation, USA).

## III. RESULTS AND DISCUSSION

### A. Inverse Scattering With Coherent Illumination

To verify the capabilities of the proposed method in quantitatively reconstructing the phase of an object through a scattering medium, objects with different phase distributions were imaged. A series of phase patterns in the  $-\pi$ – $\pi$  range, corresponding to the 0–255 grayscale, was loaded. The pixel number of each phase pattern was set to  $N \times N = 60 \times 60$ , and the pixel number of each speckle pattern was set to  $M \times M = 256 \times 256$ . Phase-type objects with phase distributions within the  $-\pi$ – $\pi$  range were retrieved first. The results are shown in Fig. 3, in which Fig. 3(a1) and (a2) show the ground truth of the objects, which correspond to four numbers and the letter “A” in different colors. Numbers 1, 2, 3, and 4 exhibit phase distributions of  $-0.5\pi$ ,  $0$ ,  $0.5\pi$ , and  $\pi$ , respectively.

Fig 3(b1), (b2) and (c1), (c2) show the reconstruction of the objects in the absence and presence of scattering medium with the calibrated TMs, respectively, in which the calibrated TM1 is measured without scatters. For a fair comparison, the other is estimated with a scattering medium. In addition, phase retrieval results by the binary-TM are also shown in Fig. 3(d1) and (d2). Obviously, although the phase of objects can be recovered behind the scattering media by binary TM, the phase distribution

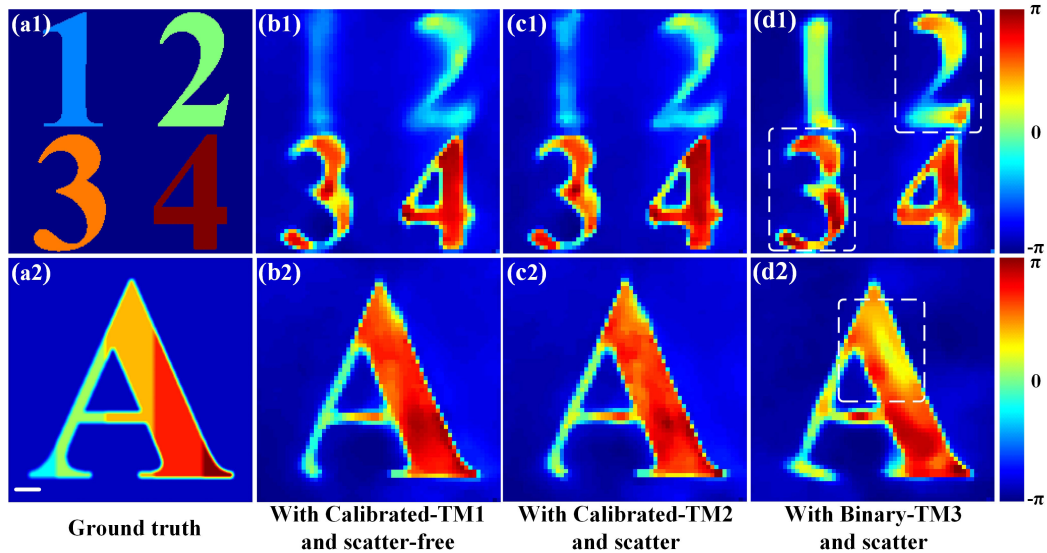


Fig. 3. Quantitative phase retrieval by using the calibrated and the binary TMs. The ground truth of the phase-type objects with different phase distributions are: (a1) Numbers from 1 to 4 corresponding to uniform phase distributions of  $-0.5\pi$ ,  $0$ ,  $0.5\pi$ , and  $\pi$ , respectively; (a2) Letter “A” with a 5-step phase distribution of  $-0.8\pi$ ,  $-0.4\pi$ ,  $0$ ,  $0.4\pi$ ,  $0.8\pi$ , from left to right. (b1) and (b2) Phase retrieval of objects distribution with calibrated-TM and scatter-free; (c1) and (c2) Phase retrieval of objects through scattering media with calibrated-TM; (d1) and (d2) Phase retrieval of objects through scattering media with binary-TM. The pixel numbers in all images are  $60 \times 60$  and the scale bar measures  $200 \mu\text{m}$ .

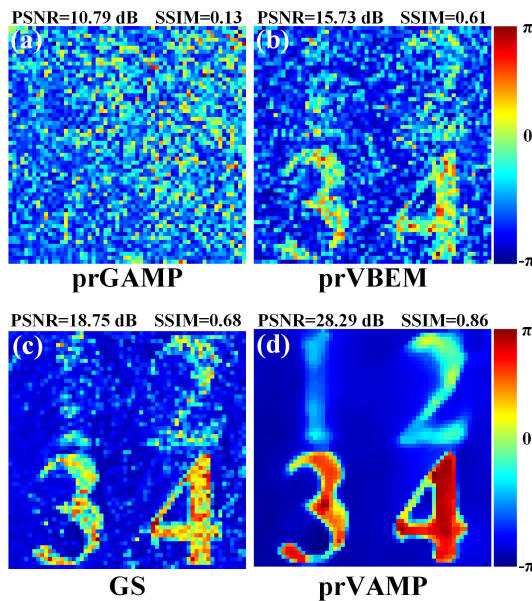


Fig. 4. Comparison of phase retrieval results through scattering media with different methods. (a)–(d) are the phase retrieval results by using prGAMP, prVBEM, the traditional iteration Gerchberg-Saxton (GS) and the prVAMP method, respectively.

is distorted and incorrect. In particular, in the selected regions (marked with white dashed lines) in Fig. 3(d1) and (d2), the phase information is chaotic when compared with Fig. 3(a) and (b). Intuitively, these results show that the proposed method is capable of quantitatively imaging a phase object behind a scattering medium, whereas the binary-TM fails to realize quantitative phase retrieval.

For quantitative evaluation, assessing via the peak-signal-to-noise-ratio (PSNR) [34] computed against the ground truth is

also performed, and the values obtained in Fig. 3(b1), (b2) and (c1), (c2) are 30.30 dB, 31.98 dB, 28.29 dB and 28.97 dB, respectively, whereas in Fig. 3 (d1), and (d2), the values are decreased to 25.05 dB and 25.84 dB, respectively. In addition, the structural similarity indexes (SSIMs) [35] that represent the difference between the imaging results and the ground truth were also calculated, and the values obtained in Fig. 3(b1), (b2) and (c1), (c2) are 0.90, 0.89, 0.86 and 0.88 (range from 0 to 1, higher is better), respectively. In Fig. 3(d1) and (d2), the values are 0.78 and 0.76, respectively. The results further demonstrate the advantages of the proposed calibrated TM in quantitative phase retrieval.

As representatives of double phase retrieval, prGAMP and prVBEM are also used to realize imaging or retrieve the phase of objects through scattering media. However, the prGAMP and prVBEM methods are sensitive to noise or limited by the coherence of illumination, leading to a lower accuracy of phase recovery, which limits their applications. Although some properties of the aforementioned methods have been compared in Ref. [31], the results of quantity phase retrieval through scattering media are absent. To further demonstrate the advantages of the proposed method, prGAMP, prVBEM and the traditional iterative Gerchberg-Saxton (GS) are selected for comparing the performance of quantified phase retrieval through scattering media. The results are shown in Fig. 4. Fig. 4(a)–(d) show the phase retrieval results through scattering media by using prGAMP, prVBME, GS and the prVAMP method, respectively. To evaluate the imaging quality, the PSNRs of the four methods are calculated, and the values are 10.79 dB, 15.73 dB, 18.75 dB and 28.29 dB, corresponding to prGAMP, prVBME, GS and the proposed prVAMP method, respectively. Again, the SSIMs of the four methods are also calculated, whose values are 0.13, 0.61, 0.68 and 0.86, respectively. Therefore, the proposed method presents advantages in both resolution

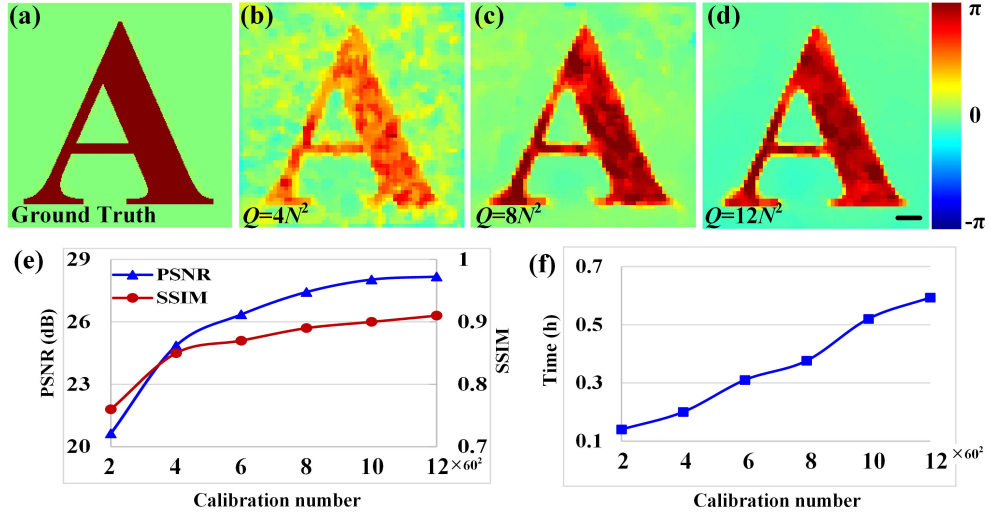


Fig. 5. Retrieved image quality for different calibration pattern numbers. (a) Ground truth of a phase target with a uniform phase distribution of  $\pi$ ; (b), (c) and (d) correspond to the retrieved imaging results with calibration pattern numbers of  $Q = 4N^2$ ,  $Q = 8N^2$ , and  $Q = 12N^2$ , respectively; (e) The trends of the PSNR and SSIM as a function of the calibration number; (f) The relationship between the TM calculating time and the calibration number. The pixel numbers in (a), (b), (c) and (d) are  $60 \times 60$  and the scale bar measures  $200 \mu\text{m}$ .

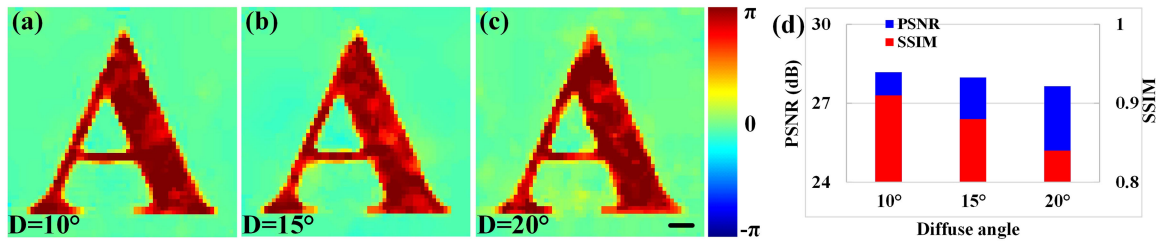


Fig. 6. Retrieved image quality for different scatters. (a), (b), and (c) correspond to the retrieved imaging results with diffusion angles of  $10^\circ$ ,  $15^\circ$ , and  $20^\circ$ , respectively; (d) The trend of the PSNR and SSIM as a function of the diffusion angle. The pixel numbers in (a), (b), (c) and (d) are  $60 \times 60$ , and the scale bar measures  $200 \mu\text{m}$ .

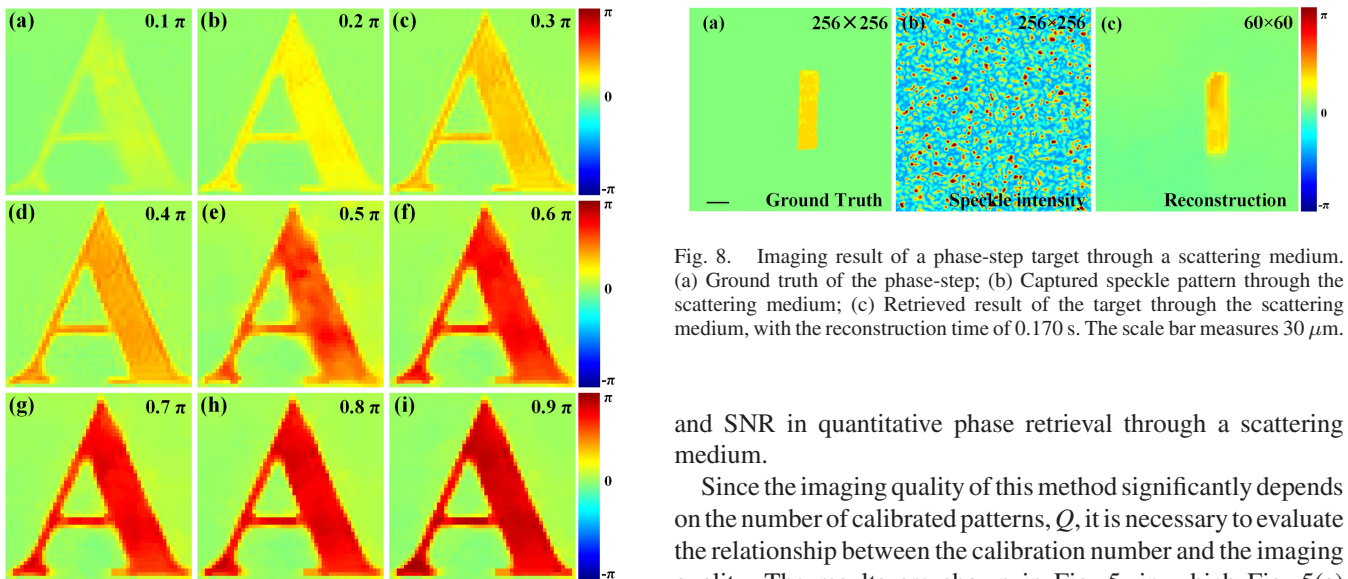


Fig. 7. Phase resolving power of the proposed method, (a)–(i) present the phase retrieval results of objects with the phase distribution from  $0.1\pi$ – $0.9\pi$  with an interval of  $0.1\pi$ .

Fig. 8. Imaging result of a phase-step target through a scattering medium. (a) Ground truth of the phase-step; (b) Captured speckle pattern through the scattering medium; (c) Retrieved result of the target through the scattering medium, with the reconstruction time of 0.170 s. The scale bar measures  $30 \mu\text{m}$ .

and SNR in quantitative phase retrieval through a scattering medium.

Since the imaging quality of this method significantly depends on the number of calibrated patterns,  $Q$ , it is necessary to evaluate the relationship between the calibration number and the imaging quality. The results are shown in Fig. 5, in which Fig. 5(a) shows the ground truth of a phase target with a uniform phase distribution of  $\pi$ , whereas Fig. 5(b)–(d) show the phase retrieval results for  $Q = 4N^2$ ,  $Q = 8N^2$ , and  $Q = 12N^2$  in calibration

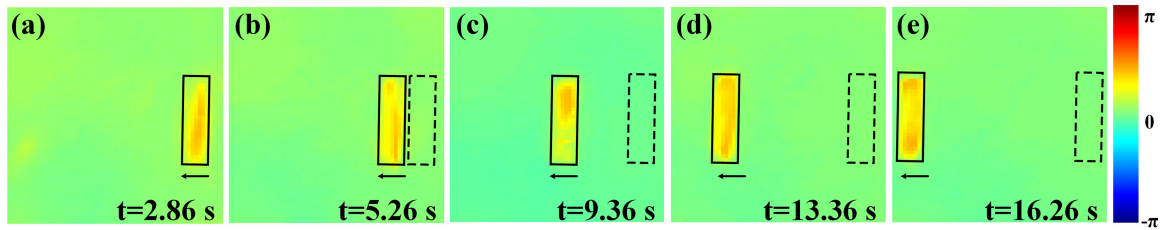


Fig. 9. Dynamic imaging results of the phase-step target through a scattering medium. (a)–(e) Retrieved time-lapsed motion process of the target. The scale bar measures  $30 \mu\text{m}$ .

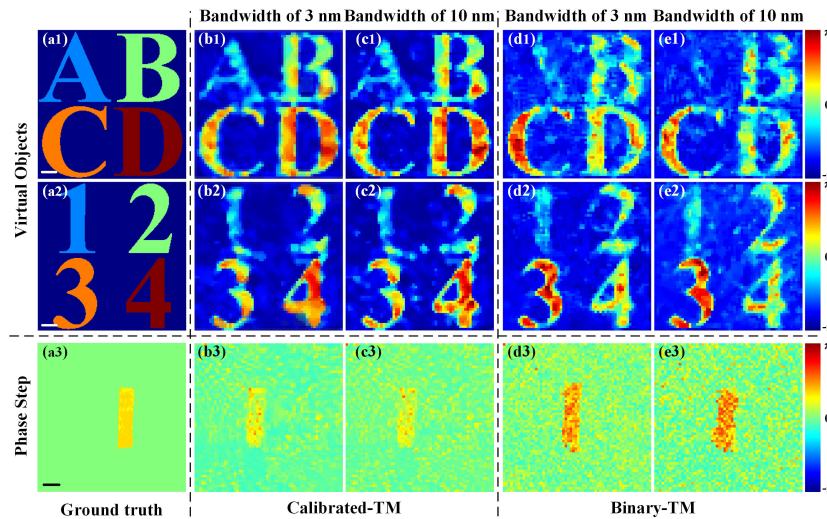


Fig. 10. Comparison of quantitative phase retrieval by using the calibrated-TMs and binary-TMs. The ground truth of the phase-type objects with different phase distributions are: (a1) Letters from A to D corresponding to uniform phase distributions of  $-0.5\pi$ ,  $0$ ,  $0.5\pi$ , and  $\pi$ , respectively; (a2) Numbers from 1 to 4 corresponding to uniform phase distributions of  $-0.5\pi$ ,  $0$ ,  $0.5\pi$ , and  $\pi$ , respectively; (a3) Ground truth of phase-step; (b1)–(b3) Phase retrieval of objects distribution with calibrated-TM under the 3 nm bandwidth laser illuminations; (c1)–(c3) Phase retrieval of objects with calibrated-TM under the 10 nm bandwidth laser illuminations; (d1)–(d3) Phase retrieval of objects with binary-TMs under the 3 nm bandwidth laser illuminations; (e1)–(e3) Phase retrieval of objects distribution with binary-TMs under the 10 nm bandwidth laser illuminations. The pixel numbers in all images are  $60 \times 60$  and the scale bar measures (a1)–(e1) and (a2)–(e2)  $200 \mu\text{m}$ , (a3)–(e3):  $30 \mu\text{m}$ .

number. To evaluate the imaging quality, the PSNRs for different calibration pattern numbers  $Q$  from  $2N^2$  to  $12N^2$ , with an interval of  $2N^2$ , are calculated, and the values obtained are 20.64 dB, 24.86 dB, 26.36 dB, 27.44 dB, 28.04 dB and 28.18 dB. In addition, the SSIMs are also calculated, and the values obtained are 0.76, 0.85, 0.87, 0.89, 0.90 and 0.91. The trends of both the PSNR and the SSIM as a function of calibration number are shown in Fig. 5(e). Fig. 5(f) shows the relationship between the calculation time of TM and the calibration number. These results show that a large number of calibration patterns give rise to a high retrieved image quality. However, the larger the number of calibration patterns is, the more time-consuming the process becomes. As a result, the  $Q = 12N^2$  dataset can be considered a good trade-off between the imaging quality and processing time.

The property of the scattering medium is another critical factor influencing the imaging quality. To evaluate this, target retrieval with different scatters and diffusion angles  $D$  of  $10^\circ$ ,  $15^\circ$ , and  $20^\circ$  are illustrated in Fig. 6(a)–(c), respectively. The values of the PSNR are 28.18 dB, 27.98 dB, and 27.65 dB, with corresponding SSIMs of 0.91, 0.88, and 0.84, respectively. Both the PSNR and SSIM curves as a function of the diffusion angle are shown in

Fig. 6(d). The phase can be successfully reconstructed from the corresponding TMs, although diffusion at large angles slightly decreases the imaging quality.

Another key factor that strongly influences the phase retrieval process is the computational time. Although the calculation of the TM is a rather time-consuming process, the GPU-accelerated algorithm enhances the measuring efficiency of the calibrated TM, and moreover, the target reconstruction is very fast. For instance, in the reconstruction of the targets shown in Figs. 3–6, the averaged consumed time are 0.191 s, 0.184 s, 0.162 s, and 0.172 s, respectively. These results show that no significant difference in the reconstruction time of different targets is observed.

In this study, the 0-255 gray value corresponding to  $-\pi$ – $\pi$  calibration patterns is used to calculate the TM; thus, a calibrated TM is acquired. In principle, it is possible to resolve an object with different phase distributions. To demonstrate the resolving ability, Fig. 7 represents the phase retrieval results of objects with a phase distribution from  $0.1\pi$ – $0.9\pi$  with an interval of  $0.1\pi$ . It is clear that with the proposed method, the phase resolving ability can reach  $0.1\pi$ .

To further demonstrate the capability of the proposed method, a phase step with a thickness of 180 nm and a refraction index of 1.55, corresponding to a phase of  $\varphi = 2\pi(n - 1)d/\lambda = 0.37\pi$  at a wavelength of 532 nm, was inserted in the target plane. The phase distribution was then reconstructed. A diffuser with a diffusion angle of  $10^\circ$  was also used. The retrieved results are shown in Fig. 8. The ground truth of the phase-step target is shown in Fig. 8(a) for comparison, and the imaging result of a speckle pattern is shown in Fig. 8(b). In this experiment, the mean value of the retrieved phase measures  $0.33\pi$ , as shown in Fig. 8(c). This result is in good agreement with the theoretical predictions. Therefore, the quantitative phase distribution of an object behind the scattering media can be successfully measured by using the proposed method.

Furthermore, the ability of the proposed method to image a dynamic target in real time was investigated. A phase step was fixed on a moving stage (KMSTS25E/M, Thorlabs, USA), and the speckle patterns were recorded during the movement. The obtained TM allows one to retrieve the target of each frame. Moreover, the dynamic imaging result of the target can be achieved by recomposing each frame in the video (see **Visualization 1**). The results are shown in Fig. 9. Here, Fig. 9(a)–(e) display the time-lapsed target motion, and the dashed and solid rectangles mark the starting and current positions of the target at a given moment, respectively, along the direction marked by the arrow. The results show that real-time imaging of a phase target behind a scattering medium was successfully achieved.

### B. Inverse Scattering With Partial Coherent Illumination

It is worth noting that the proposed method can also work under partial coherent illumination. To verify this, a supercontinuum laser source (SC-5, YSL Photonics, Inc., China) and bandpass filters (with bandwidths of 3 nm and 10 nm at center wavelength  $\lambda = 532$  nm) were combined to select the proper wavelength for illumination. The calibrated TM and the binary TM are acquired first, and then objects with different phase distributions are retrieved quantitatively.

The results are shown in Fig. 10, where Fig. 10(a1) and (a2) show the ground truth of the objects, which correspond to four numbers and four letters. Again, the numbers 1, 2, 3, and 4 and A, B, C and D exhibit phase distributions of  $-0.5\pi$ ,  $0$ ,  $0.5\pi$ , and  $\pi$ , respectively. Fig. 10(a3) shows the ground truth of a phase step. Fig. 10(b1)–(b3) and (c1)–(c3) show the reconstruction of the objects with the calibrated TMs under 3 nm and 10 nm bandwidth illumination, respectively. The results demonstrate the ability to perform quantity phase retrieval by the calibrated TM, although the bandwidth slightly decreases the imaging quality. In contrast, Fig. 10(d1)–(d3) and (e1)–(e3) show the reconstruction of the objects with binary TM under 3 nm and 10 nm bandwidth laser illumination, respectively. Similar to the imaging results with coherent illumination, the phase information retrieved by the binary TM is distorted. Again, the PSNRs of Fig. 10(b3)–(e3) are selected and calculated to evaluate the imaging quality, and

the values are 23.84 dB, 22.87 dB, 20.37 dB and 19.42 dB, respectively. This implies that the ability of traditional binary-TM in quantity phase retrieval is absent, whereas one can recover the phase information by the proposed calibrated-TM method.

## IV. CONCLUSION

In this study, a CS method to quantify the TM of an imaging system containing a scattering medium was reported. The TM based on a generalized linear model of an imaging system with a scattering medium can be obtained by using a series of calibration images. Then, both commonly used virtual objects and practical phase targets with specific optical thicknesses are imaged and analyzed to evaluate the performance of the proposed method. The imaging performances of the calibrated TM are further compared with those of the binary TM method, both in coherent and partially coherent illumination, which further shows the advantages of calibrated TM in quantitative phase retrieval. The proposed method can extract the phase information of objects hidden behind a scattering medium without special requirements on the medium. Therefore, it can be applied in related imaging fields where the object phase information needs retrievable behind/within the scattering medium.

## REFERENCES

- [1] A. P. Mosk, A. Lagendijk, G. Leroosey, and M. Fink, "Controlling waves in space and time for imaging and focusing in complex media," *Nature Photon.*, vol. 6, pp. 283–292, May 2012.
- [2] A. K. Singh, D. N. Naik, G. Pedrini, M. Takeda, and W. Osten, "Exploiting scattering media for exploring 3D objects," *Light: Sci. Appl.*, vol. 6, Sep. 2017, Art. no. e16219.
- [3] R. Horstmeyer, H. Ruan, and C. Yang, "Guidestar-assisted wavefront-shaping methods for focusing light into biological tissue," *Nature Photon.*, vol. 9, pp. 563–571, Aug. 2015.
- [4] H. Yu *et al.*, "Recent advances in wavefront shaping techniques for biomedical applications," *Curr. Appl. Phys.*, vol. 15, pp. 632–641, May 2015.
- [5] S. Yoon *et al.*, "Deep optical imaging within complex scattering media," *Nature Rev. Phys.*, vol. 2, pp. 141–158, Feb. 2020.
- [6] V. Bianco, M. Paturzo, A. Finizio, K. A. Stetson, and P. Ferraro, "Portable IR laser system for real-time display of alive people in fire scenes," *J. Disp. Technol.*, vol. 11, pp. 834–838, Oct. 2015.
- [7] T. Čížmár, M. Mazilu, and K. Dholakia, "In situ wavefront correction and its application to micromanipulation," *Nature Photon.*, vol. 4, pp. 388–394, May 2010.
- [8] I. M. Vellekoop and A. P. Mosk, "Focusing coherent light through opaque strongly scattering media," *Opt. Lett.*, vol. 32, pp. 2309–2311, Aug. 2007.
- [9] O. Katz, P. Heidmann, M. Fink, and S. Gigan, "Non-invasive single-shot imaging through scattering layers and around corners via speckle correlations," *Nature Photon.*, vol. 8, pp. 784–790, Aug. 2014.
- [10] S. Xu *et al.*, "Ultrafast optical Kerr gate of bismuth–plumbum oxide glass for time-gated ballistic imaging," *J. Mod. Opt.*, vol. 61, pp. 1452–1456, Jul. 2014.
- [11] I. Freund, M. Rosenbluh, and S. Feng, "Memory effects in propagation of optical waves through disordered media," *Phys. Rev. Lett.*, vol. 61, Nov. 1988, Art. no. 2328.
- [12] O. Katz, E. Small, and Y. Silberberg, "Looking around corners and through thin turbid layers in real time with scattered incoherent light," *Nature Photon.*, vol. 6, pp. 549–553, Jul. 2012.
- [13] W. J. Choi, D. I. Jeon, S. G. Ahn, J. H. Yoon, S. Kim, and B. H. Lee, "Full-field optical coherence microscopy for identifying live cancer cells by quantitative measurement of refractive index distribution," *Opt. Exp.*, vol. 18, pp. 23285–23295, Oct. 2010.
- [14] E. Watanabe, T. Hoshiba, and B. Javid, "High-precision microscopic phase imaging without phase unwrapping for cancer cell identification," *Opt. Lett.*, vol. 38, pp. 1319–1321, Apr. 2013.

- [15] C. S. Guo, Y. N. Yu, X. T. Zhang, J. R. Zhao, and H. Jiang, "Three-dimensional coordinate measurements using a multiple-pinhole interferometer," *Opt. Lett.*, vol. 36, pp. 2260–2262, Jun. 2011.
- [16] C. L. Hsieh, Y. Pu, R. Grange, G. Laporte, and D. Psaltis, "Imaging through turbid layers by scanning the phase conjugated second harmonic radiation from a nanoparticle," *Opt. Exp.*, vol. 18, pp. 20723–20731, Sep. 2010.
- [17] C. Ma, X. Xu, Y. Liu, and L. V. Wang, "Time-reversed adapted-perturbation (TRAP) optical focusing onto dynamic objects inside scattering media," *Nature Photon.*, vol. 8, pp. 931–936, Dec. 2014.
- [18] A. K. Singh, D. N. Naik, G. Pedrini, M. Takeda, and W. Osten, "Looking through a diffuser and around an opaque surface: A holographic approach," *Opt. Exp.*, vol. 22, pp. 7694–7701, Apr. 2014.
- [19] R. K. Singh, A. M. Sharma, and B. Das, "Quantitative phase-contrast imaging through a scattering media," *Opt. Lett.*, vol. 39, pp. 5054–5057, Sep. 2014.
- [20] S. Kodama *et al.*, "Three-dimensional microscopic imaging through scattering media based on in-line phase-shift digital holography," *Appl. Opt.*, vol. 58, pp. G345–G350, Dec. 2019.
- [21] S. Popoff, G. Lerosey, M. Fink, A. C. Boccarda, and S. Gigan, "Controlling light through optical disordered media: Transmission matrix approach," *New J. Phys.*, vol. 13, Dec. 2011, Art. no. 123021.
- [22] A. Boniface, M. Mounaix, B. Blochet, R. Piestun, and S. Gigan, "Transmission-matrix-based point-spread-function engineering through a complex medium," *Optica*, vol. 4, pp. 54–59, Jan. 2017.
- [23] S. Popoff, G. Lerosey, M. Fink, A. C. Boccarda, and S. Gigan, "Image transmission through an opaque material," *Nature Commun.*, vol. 1, no. 6, Sep. 2010, Art. no. 81.
- [24] S. M. Popoff, G. Lerosey, R. Carminati, M. Fink, A. C. Boccarda, and S. Gigan, "Measuring the transmission matrix in optics: An approach to the study and control of light propagation in disordered media," *Phys. Rev. Lett.*, vol. 10, Mar. 2010, Art. no. 100601.
- [25] A. Boniface, J. Dong, and S. Gigan, "Non-invasive focusing and imaging in scattering media with a fluorescence-based transmission matrix," *Nature Commun.*, vol. 11, Dec. 2020, Art. no. 6154.
- [26] A. Drémeau *et al.*, "Reference-less measurement of the transmission matrix of a highly scattering material using a DMD and phase retrieval techniques," *Opt. Exp.*, vol. 23, pp. 11898–11911, May 2015.
- [27] M. Zhao, M. J. Zhao, H. D. Wu, and W. H. Xu, "Phase object retrieval through scattering medium," *J. Opt.*, vol. 20, no. 5, Apr. 2018, Art. no. 055602.
- [28] B. Rajaei, E. W. Tramel, S. Gigan, F. Krzakala, and L. Daudet, "Intensity-only optical compressive imaging using a multiply scattering material and a double phase retrieval approach," in *Proc. IEEE Int. Conf. Acoust., Speech, Signal Process.*, Shanghai, China, 2016, pp. 4054–4058.
- [29] P. Schniter and S. Rangan, "Compressive phase retrieval via generalized approximate message passing," *IEEE Trans. Signal Process.*, vol. 63, no. 4, pp. 1043–1055, Feb. 2015.
- [30] A. Drémeau and F. Krzakala, "Phase recovery from a Bayesian point of view: The variational approach," in *Proc. IEEE Int. Conf. Acoust., Speech Signal Process.*, South Brisbane, QLD, Australia, 2015, pp. 3661–3665.
- [31] C. A. Metzler, M. K. Sharma, S. Nagesh, R. G. Baraniuk, O. Cossairt, and A. Veeraraghavan, "Coherent inverse scattering via transmission matrices: Efficient phase retrieval algorithms and a public dataset," in *Proc. IEEE Int. Conf. Comput. Photogr.*, Stanford, CA, USA, 2017, pp. 1–16.
- [32] M. K. Sharma, C. A. Metzler, S. Nagesh, O. Cossairt, R. G. Baraniuk, and A. Veeraraghavan, "Inverse scattering via transmission matrices: Broadband illumination and fast phase retrieval algorithms," *IEEE Trans. Comput. Imag.*, vol. 6, pp. 95–108, 2020.
- [33] P. Schniter, S. Rangan, and A. K. Fletcher, "Vector approximate message passing for the generalized linear model," in *Proc. 50th Asilomar Conf. Signals, Syst. Comput.*, 2016, pp. 1525–1529.
- [34] Q. Huynh-Thu and M. Ghanbari, "Scope of validity of PSNR in image/video quality assessment," *Electron. Lett.*, vol. 44, pp. 800–802, Jun. 2008.
- [35] Z. Wang, A. C. Bovik, H. R. Sheikh, and E. P. Simoncelli, "Image quality assessment: From error visibility to structural similarity," *IEEE Trans. Image Process.*, vol. 13, no. 4, pp. 600–612, Apr. 2004.